2015

Numerical Dissipation Control in High Order Shock-Capturing Schemes for LES of Low Speed Flows

D. V. Kotov
Bay Area Environmental Research Institute, dmitry.v.kotov@nasa.gov

Helen C. Yee
NASA Ames Research Center, yee@nas.nasa.gov

Alan A. Wray
NASA Ames Research Center, alan.a.wray@nasa.gov

Bjorn Sjögreen
Lawrence Livermore National Laboratories, sjogreen2@llnl.gov

Numerical Dissipation Control in High Order Shock-Capturing Schemes for LES of Low Speed Flows

D.V. Kotov, H.C. Yee, A.A. Wray, and B. Sjögreen

Abstract In Kotov et al. (Proceedings of ICCFD8, 2014) the LES of a turbulent flow with a strong shock by Yee and Sjögreen (Proceedings of ICOSAHOM 09, Trondheim, Norway, 2013) scheme indicated a good agreement with the filtered DNS data. There are vastly different requirements in the minimization of numerical dissipation for accurate turbulence simulations of different compressible flow types and flow speeds. The present study examines the versatility of the Yee and Sjögreen scheme for LES of low speed flows. Special attention is focused on the accuracy performance of this scheme using the Smagorinsky and the Germano-Lilly SGS models.

1 Introduction

For the last decade, high order shock-capturing methods with numerical dissipation controls have been the state-of-the-art numerical approach for direct numerical simulation (DNS) and large eddy simulation (LES) of turbulent flows with shocks. See for example [1–10]. The majority of these methods involve flow sensors with parameter tuning applied depending on the flow type. Some of the flow sensors were designed for certain flow types and might not preserve their high accuracy when used to simulate a different flow type. In a study presented in Johnsen et al. [3], all of the shock-capturing schemes involve tuning of the parameters. It appears that the Yee and Sjogreen filter scheme is not as accurate as the hybrid scheme presented in [3] as the key parameter κ responsible for minimizing the numerical

D.V. Kotov (✉)
Bay Area Environmental Research Institute, Petaluma, CA 94952, USA
e-mail: dmitry.v.kotov@nasa.gov; dmitry.kotov84@gmail.com

H.C. Yee • A. Wray
NASA Ames Research Center, Moffett Field, CA 94035, USA
e-mail: helen.m.yee@nasa.gov; Alan.A.Wray@nasa.gov

B. Sjögreen
Lawrence Livermore National Laboratory, Livermore, CA 94551, USA
e-mail: sjogreen2@llnl.gov

R.M. Kirby et al. (eds.), *Spectral and High Order Methods for Partial Differential Equations ICOSAHOM 2014*, Lecture Notes in Computational Science and Engineering 106, DOI 10.1007/978-3-319-19800-2_25

dissipation in the 2007 Yee and Sjogreen scheme [4] was mandated to set to a constant for all of test cases shown for results presented in [3]. See [2, 5] for a description of better control of numerical dissipation using a local κ. The hybrid scheme presented in [3] which employed the Ducros et al. flow sensor [6] also consists of a key tuning parameter δ. From our study presented below of the same Taylor-Green vortex problem considered in [3], the cut-off parameter δ to be 1 to achieve the best accurate result. On the other hand, for the isotropic turbulence with shocklets test case, the Ducros et al. flow sensor δ parameter has to be reduced, mostly by trial and error. Yet in another study [1] for turbulence interacting with a high speed stationary shock, depending on the Mach number and turbulent Mach number, different δ are required for each case.

In recognizing the different requirements on numerical dissipation control for DNS and LES of a variety of compressible flow types, Yee and Sjogreen, [2], presented a general framework for a local κ and the accompanying variety of flow sensors were introduced into their high order nonlinear filter scheme. Aside from suggesting different local κ formulation, Yee and Sjogreen also proposed the use of a combination of different flow sensors. Their proposed scheme with numerical dissipation control has not been studied extensively. A subset to the sequel to [2] was presented in [5]. This is yet another sequel to Yee and Sjogreen. The goal of this work is to examine the different combinations of flow sensors for DNS and LES of low speed turbulent flows.

2 High Order Nonlinear Filter Schemes

This section gives a brief overview of the high-order nonlinear filter scheme of Yee et al. [2, 4, 5, 7] for accurate computations of DNS and LES of compressible turbulence for a wide range of flow types by introducing as little shock-capturing numerical dissipation as possible.

Preprocessing Step Before the application of a high-order non-dissipative spatial base scheme, a preprocessing step is employed to improve numerical stability. The inviscid flux derivatives of the governing equations are split into the following three ways, depending on the flow types and the desire for rigorous mathematical analysis or physical argument.

- Entropy splitting of [8]. This is non-conservative and the derivation is based on the physical entropy variable and energy norm stability for the compressible Euler equations with boundary closure for the initial boundary value problem.
- The Ducros et al. splitting [9] for systems. This is a conservative splitting and the derivation is based on physical arguments.
- Tadmor entropy conservation formulation for systems [10]. The derivation is based on mathematical analysis. Preliminary study in [10] indicated the Tadmor entropy conservation formulation is more diffusive than the other two splittings.

Base Scheme Step A full time step is advanced using a high-order non-dissipative spatially central scheme on the split form of the governing equations. A summation-by-parts (SBP) boundary operator [11] and matching order conservative high-order free stream metric evaluation for curvilinear grids [12] are used. Note that the base scheme can be a high order compact scheme [13], the standard high order central schemes or spectral methods. However the same entropy stable SBP boundary closure for high order central schemes is not valid for the latter base schemes.

Post-Processing (Nonlinear Filter Step) To further improve the accuracy of the computed solution from the base scheme step, after a full time step of a base scheme step the post-processing step is used to nonlinearly filter the solution by a dissipative portion of a high-order shock-capturing scheme with a local flow sensor. The flow sensor provides locations and amounts of built-in shock-capturing dissipation that can be further reduced or eliminated. At each grid point a local flow sensor is employed to analyze the regularity of the computed flow data. Only the strong discontinuity locations would receive the full amount of shock-capturing dissipation. In smooth regions no shock-capturing dissipation would be added, unless high frequency oscillations are developed, owning to the possibility of numerical instability in long time integrations of nonlinear governing PDEs. In regions with strong turbulence, if needed, a small fraction of the shock-capturing dissipation would be added to improve stability. Note that the filter numerical fluxes only involve the inviscid flux derivatives regardless if the flow is viscous or inviscid. If viscous terms are present, a matching high order central difference operator (as the inviscid difference operator) is included on the base scheme step.

Let U^* be the solution after the completion of the full time step of the base scheme step. The final update of the solution after the filter step is (with the numerical fluxes in the y- and z-directions suppressed as well as their corresponding y- and z-direction indices on the x inviscid flux suppressed)

$$U_{j,k,l}^{n+1} = U_{j,k,l}^* - \frac{\Delta t}{\Delta x}[H_{j+1/2}^* - H_{j-1/2}^*], \quad H_{j+1/2}^* = R_{j+1/2}\overline{H}_{j+1/2}, \tag{1}$$

where $R_{j+1/2}$ is the matrix of right eigenvectors of the Jacobian of the inviscid flux vector in terms of Roe's average states based on U^*. $H_{j+1/2}^*$ and $H_{j-1/2}^*$ are "filter" numerical fluxes in terms of Roe's average states based on U^*. Denote the elements of $\overline{H}_{j+1/2}$ by $\overline{h}_{j+1/2}^l, l = 1, 2, \ldots, 5$, where

$$\overline{h}_{j+1/2}^l = \frac{\kappa_{j+1/2}^l}{2} w_{j+1/2}^l \phi_{j+1/2}^l. \tag{2}$$

Here $w_{j+1/2}^l$ is a flow sensor to activate the nonlinear numerical dissipation portion of a high order shock-capturing scheme $\frac{1}{2}\phi_{j+1/2}^l$, and $\kappa_{j+1/2}^l$ is a flow dependent positive parameter to control the amount of shock-capturing dissipation to be used. The nonlinear dissipative portion of a high-resolution shock-capturing scheme "$\frac{1}{2}\phi_{j+1/2}^l$" can be any shock-capturing scheme. The choice of the parameter $\kappa_{j+1/2}^l$

can be different for different flow types and is automatically chosen by using the local $\kappa^l_{j+1/2}$ described in [2]. The flow sensor $w^l_{j+1/2}$ can be a variety of formulae introduced in the literature or can be switched from one flow sensor to another, depending on the computed flow data at that particular location. For a variety of local flow sensors with automatic selection of the proper parameter, depending on different flow type, see [2]. The form of Tauber-Sandham [14] for the filter numerical flux uses the Ducros et al. flow sensor as $\kappa^l_{j+1/2}$ and the Harten artificial compression method formula (ACM) as the flow sensor indicated in [7] and similarly in [15] are part of the Yee and Sjögreen adaptive numerical dissipation control generalization filter formulae. The form of Ducros et al. flow sensor is $w = (\nabla \mathbf{u})^2/\big((\nabla \mathbf{u})^2 + \omega^2 + \varepsilon\big)$. Here $\mathbf{u}$ is the velocity vector, ω is the vorticity magnitude and ε is a small number to avoid division by zero (e.g., 10^{-6}). The Ducros et al. flow sensor consists of a cut off parameter δ that can be used to switch on or off the dissipative portion of the high order shock-capturing scheme. If δ is set to be one, the dissipation only switches on when it encounters a shock wave. For lower value of the cut off δ parameter, vorticity can be detected.

The current numerical experimental study is confined to the following four forms for the filter numerical flux. It is well known that for certain low speed turbulence flows, the schemes of choice are spectral and high order compact, or central schemes with SBP boundary closures. The nonlinear filter step is not needed and this option using the high order central scheme base scheme only is included as the fifth scheme for comparison (the last bullet below).

- The first form of the filter numerical flux indicated in [2] is where $\kappa^l_{j+1/2}$ is the Mach curve for low speed flow described in [2]. $w_{j+1/2}$ is the wavelet flow sensor. If the tenth-order central base scheme, entropy splitting and the dissipative portion of the ninth-order WENO scheme (WENO9) are employed, it is denoted by WENO9fi-Esplit-Wav $\kappa(i)$. If the Ducros et al. splitting is used, it is denoted by WENO9fi-Dsplit-Wav.
- The second form of the numerical flux is the same as the first form except $\kappa^l_{j+1/2}$ is a constant based on the initial Mach number of the flow. The corresponding schemes are denoted by Esplit-Wav $\kappa = const$ and WENO9fi-Dsplit-Wav $\kappa = const$
- The third form of the numerical flux is where $\kappa^l_{j+1/2}$ is a positive non-zero constant, and $w_{j+1/2}$ is the Ducros et al. flow sensor in conjunction with the δ cut off parameter. The corresponding schemes are denoted by WENO9fi-Esplit-Ducr & WENO9fi-Dsplit-Ducr.
- The fourth form of the numerical flux is where the Ducros et al. flow sensor is used as $\kappa^l_{j+1/2}$, and $w_{j+1/2}$ is the wavelet flow sensor or the ACM flow sensor. For the same base scheme and the dissipative portion of WENO9, it is denoted by WENO9fi-Esplit-WavD & WENO9fi-Dsplit-WavD (WENO9fi-Esplit-AcmD & WENO9fi-Dsplit-AcmD).
- The last form is when no nonlinear filter step is used, i.e., only the base scheme step is employed. It is denoted by C10-Esplit in the case of employing the tenth-order central base scheme with entropy splitting. If the Ducros et al. splitting is used, it is denoted by C10-Dsplit.

The subgrid-scale (SGS) Smagorinsky model denoted by LES1 using $C_s = 0.0085$ [16] and the dynamic Germano model [17, 18] denoted by LES2 are considered. All of the results shown use the third-order Runge-Kutta temporal discretization.

3 Test Cases

This section illustrates the performance of our high-order filter scheme for DNS and LES of two 3D low speed turbulence flows considered in [3]. The first test case is the nearly incompressible (inviscid) Taylor-Green vortex problem and its viscous counterpart. The second test case is the decay of an isotropic turbulence with shocklets for an initial turbulent Mach number $M_{t,0} = 0.6$. For both test cases grid convergence studies are performed using uniform 256^3, 128^3 and 64^3 grids for the DNS simulations. Grid convergence studies also are performed using uniform 128^3, 64^3 and 32^3 grids for LES computations. Studies found that for an accurate numerical dissipation control scheme, a coarse grid DNS using a uniform 64^3 grid compared well with the filtered DNS using a fine grid of 256^3 grid points (spectrally filtered to a 64^3 grid). For the LES computations the 32^3 grid is too coarse for obtaining an accurate solution, whereas, the 128^3 grid solutions are almost on top of the filtered DNS computation on the 256^3 grid. Here, only the results using the 64^3 are briefly discussed. Due to a page limitation, see [19] for extended comparisons with more relevant illustrations that are not able to include here.

Taylor-Green Vortex: The 3D compressible inviscid test case solve the Euler equations with gas constant $\gamma = 5/3$. The computational domain is a 2π square cube using a uniform 64^3 grid. Boundary conditions are periodic in all directions. The initial conditions are:

$$\begin{aligned} &\rho = 1, \quad p = 100 + ([\cos(2z) + 2][\cos(2x) + \cos(2y)] - 2)/16, \\ &u_x = \sin x \cos y \cos z, \quad u_y = -\cos x \sin y \cos z, \quad u_z = 0. \end{aligned} \tag{3}$$

The initial turbulent Mach number is $M_{t,0} = 0.042$ and the final time is $t = 10$. We also consider the viscous counterpart of the Taylor-Green vortex problem. In the viscous case the physical viscosity is assumed to follow a power-law: $\mu/\mu_{ref} = \left(T/T_{ref}\right)^{3/4}$. Here we use $\mu_{ref} = 0.005$ and $T_{ref} = 1$ in non-dimensional units. The initial Reynolds number is $Re_0 = 2040$. For this low-Mach number flow without high shear regime the simulation actually does not require any numerical dissipation. However, we use the same shock-capturing scheme with adaptive numerical dissipation control to demonstrate its accurate performance for such low-Mach number cases. The key study involves the assessment of accuracy of the computed solution using different forms of $\kappa^l_{j+1/2}$ and different values of δ mentioned above.

Inviscid Taylor-Green Vortex—DNS Scheme Comparison: In the inviscid case the kinetic energy should be constant. It can be used as a criterion to judge the accuracy of the four considered filter numerical fluxes. The coarse grid DNS (64^3 grid—no SGS model) comparison among different methods by examining the temporal evolution of the mean kinetic energy and enstrophy comparing with the 256^3 grid filtered DNS reference solution (figure not shown). The preservation of kinetic energy is achieved with C10-split, WENO9fi-Dsplit-WavD and WENO9fi-Dsplit-Wav $\kappa = 10^{-5}$, while WENO9fi-Dsplit-Wav $\kappa(i)$ obtains a small loss in energy after $t \approx 6$. All four methods presented on the enstrophy plot demonstrate good agreement with the semi-analytical solution [20], which is defined on the interval $0 \leq t \leq 3.5$. The enstrophy values obtained using WENO9fi-Dsplit-Wav $\kappa(i)$ are slightly smaller than those obtained using the other three methods.

Viscous Taylor-Green Vortex—DNS and LES Scheme Comparison: The temporal evolution of the mean-square velocity and enstrophy of the coarse grid DNS (no SGS model) results on a 64^3 grid by different methods are shown in [19] The reference solution is the DNS simulation using a 256^3 grid and spectral filtering to the 64^3 grid. For this viscous case the most accurate cut off parameter δ in WENO9fi-Esplit-WavD and WENO9fi-Dsplit-Ducr is when $\delta = 1$. The kinetic energy computed solutions by all considered methods matches the reference solution. The difference between methods is only visible on the enstrophy comparison, though all the results are very close to the reference solution. The methods using Ducros et al. split C10-Dsplit and WENO9fi-Dsplit-Wav $\kappa = 10^{-5}$ as well as WENO9fi-Esplit-Wav $\kappa(i)$ obtain slightly more accurate results than C10-Esplit and WENO9fi-Esplit-WavD.

The results obtained using the LES1 model is shown in Fig. 1. Results obtained in LES1 are closer to the reference solution than the results obtained using the dynamic model LES2 (figure not shown; see [19]). All LES methods underestimate both the

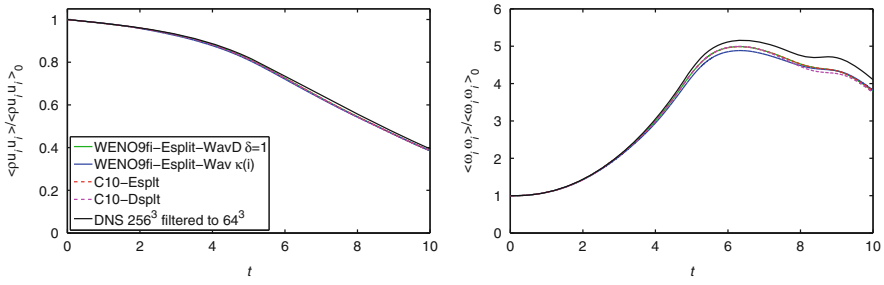

Fig. 1 LES1 comparison for the viscous Taylor-Green vortex problem using a 64^3 grid: Temporal evolution of the kinetic energy (*left*) and enstrophy (*right*). The reference solution is the DNS computation on a 256^3 grid and spectrally filtered to a 64^3 grid

kinetic energy and the enstrophy. WENO9fi-Esplit-Wav $\kappa(i)$ is slightly less accurate than C10-Dsplit and WENO9fi-Esplit-WavD. The accuracy by C10-Esplit and C10-Dsplit are almost the same.

Decaying Isotropic Turbulence with Shocklets: The second test case is the decaying compressible isotropic turbulence with eddy shocklets considered in [3]. For high enough turbulent Mach number, M_t weak shock waves (shocklets) develop spontaneously from the turbulent motions. For the current numerical experiment we set the initial $M_{t,0} = 0.6$. The filtered governing equations are solved using gas constant $\gamma = 1.4$. The computational domain is on the $2\pi^3$ cube with periodic boundary conditions in all directions. The physical viscosity is assumed to follow a power-law.

The initial condition consists of a random solenoidal velocity field $u_{i,0}$ that satisfies $E(k) \sim k^4 \exp(-2(k/k_0)^2)$, $\frac{3}{2}u_{rms,0}^2 = \frac{\langle u_{i,0}u_{i,0}\rangle}{2} = \int_0^\infty E(k)dk$. The brackets here denote averaging over the entire computational domain. For this study we put $u_{rms,0} = 1$ and $k_0 = 4$. The density and pressure fields are initially constant with initial turbulent Mach number $M_{t,0} = 0.6$ and Taylor-scale Reynolds $Re_{\lambda,0} = 100$. These parameters are defined as follows: $M_t = \frac{\sqrt{\langle u_i u_i\rangle}}{\langle c\rangle}$, $Re_\lambda = \frac{\langle\rho\rangle u_{rms}\lambda}{\langle\mu\rangle}$, $u_{rms} = \sqrt{\frac{\langle u_i u_i\rangle}{3}}$, $\lambda = \sqrt{\frac{\langle u_x^2\rangle}{\langle(\partial_x u_x)^2\rangle}}$. The time scale is $\tau = \lambda_0/u_{rms,0}$ and the final time is $t/\tau = 4$. The final turbulent Mach number is $M_t = 0.29$.

Unlike the Taylor-Green vortex case, the most accurate solutions are obtained using a smaller κ and for vales of δ between 0.7 and 1. Comparisons of the temporal evolutions of the mean-square velocity, enstrophy, temperature variance and dilatation using by the various filter numerical fluxes on a 64^3 coarse grid DNS (no SGS model) are shown in [19]. The reference solution was obtained from the DNS simulation using a 256^3 grid and spectral filtering to a 64^3 grid (digitized from [3]). The best results are obtained with C10-AV12, WENO9fi-Dsplit-Wav $\kappa(i)$ and WENO9fi-Esplit-Ducr. The cut-off parameter of the Ducros et al. sensor in WENO9fi-Esplit-WavD is $\delta = 0.7$. However, the results remain almost the same when δ increases slightly beyond 0.7. For the dilatation, the best match with the reference solution is obtained by method C10-AV12 . However, this scheme underestimates the enstrophy, while the rest of the methods either match or slightly overestimate the enstrophy. The results obtained using the LES1 model is shown in Fig. 2. The LES1 computations are closer to the reference solution than the dynamic model LES2 (figure not shown). The best results is obtained with C10-Esplit, WENO9fi-Esplit-Ducr and WENO9fi-Esplit-WavD. The spectra of this isotropic decaying turbulence test case were examined, the computed spectra by these schemes are as expected and results are not shown due to a space limitation. See [19] for the comparison.

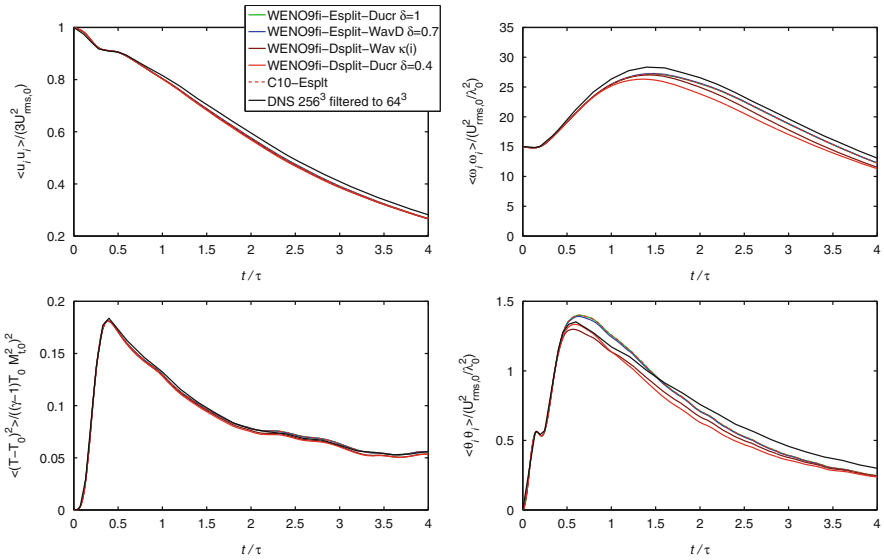

Fig. 2 LES1 comparison for the isotropic turbulence problem using a 64^3 grid: Temporal evolution of kinetic energy (*top left*), enstrophy (*top right*), temperature variance (*bottom left*) and dilatation, $\theta_i = \partial_i u_i$ (*bottom right*). The reference solution is the digitized solution from [3] on a 256^3 grid spectrally filtered to a 64^3 grid

4 Conclusions

The performance of the filter scheme with different flow sensors was demonstrated in LES and DNS of low-Mach number flows. Forms (1)–(4) for the filter numerical flux were chosen to demonstrate that for low speed turbulence flows without strong shear waves, the constant κ vs. the local $\kappa^l_{j+1/2}$ behave similarly. The main difference when using the constant κ parameter is that one has to know the flow structure of the entire evolution a priori in order to select the proper constant κ parameter. Contrary to the considered low speed flow test cases, our previous investigations [2, 5, 7, 21–24] for various complex high speed shock-turbulence interaction flows, employing the local $\kappa^l_{j+1/2}$ would provide an automatic selection of the amount of numerical dissipation needed at each flow location, thus, leading to a more accurate DNS and LES simulation with less tuning of parameters.

References

1. D. Kotov, H.C. Yee, A. Hadjadj, A. Wray, B. Sjögreen, in *Proceedings of ICCFD8* (Chengdu, Sichuan, China; also expanded version submitted to CiCP, 2014, 2014)
2. H.C. Yee, B. Sjögreen, in *Proceedings of ICOSAHOM 09* (Trondheim, Norway, 2013)

3. E. Johnsen, J. Larsson, A. Bhagatwala, W. Cabot, P. Moin, B. Olson, P. Rawat, S. Shankar, B. Sjögreen, H. Yee, X. Zhong, S. Lele, J. Comput. Phys. **229**, 1213 (2010)
4. H.C. Yee, B. Sjögreen, J. Comput. Phys. **225**, 910 (2007)
5. D. Kotov, H.C. Yee, B. Sjögreen, in *Proceedings of the ASTRONUM-2013* (Biarritz, France, 2013)
6. F. Ducros, V. Ferrand, F. Nicoud, C. Weber, D. Darracq, C. Gacherieu, T. Poinsot, J. Comput. Phys. **152**, 517 (1999)
7. H.C. Yee, N. Sandham, M. Djomehri, J. Comput. Phys. **150**, 199 (1999)
8. H.C. Yee, M. Vinokur, M. Djomehri, J. Comput. Phys. **162**, 33 (2000)
9. F. Ducros, F. Laporte, T. Soulères, V. Guinot, P. Moinat, B. Caruelle, J. Comput. Phys. **161**, 114 (2000)
10. B. Sjögreen, H.C. Yee, in *Proceedings of the 8th European Conference on Numerical Mathematics & Advanced Applications (ENUMATH 2009)* (Uppsala University, Uppsala, Sweden, 2009)
11. B. Sjögreen, H.C. Yee, in *Proceedings of the Turbulence and Shear Flow Phenomena 5 (TSFP-5)* (Munich, Germany, 2007)
12. B. Sjögreen, H.C. Yee, M. Vinokur, J. Comput. Phys. **265**, 211 (2014)
13. M. Ciment, Leventhal, Math. Comput. **29**, 985 (1975)
14. E. Touber, N. Sandham, Shock Waves **19**(6), 469 (2011)
15. S.C. Lo, G. Blaisdell, A. Lyrintzis, J. Numer. Methods Fluids **62**(5), 473 (2010)
16. G. Erlebacher, M.Y. Hussaini, C.G. Speziale, T.A. Zang, J. Fluid Mech. **238**, 155 (1992)
17. M. Germano, U. Piomelli, P. Moin, W. Cabot, Phys. Fluids **3**(7), 1760 (1991)
18. D.K. Lilly, Phys. Fluids **4**(3), 633 (1992)
19. D.V. Kotov, H.C. Yee, A. Wray, B. Sjögreen, Annual Research Briefs, Center for Turbulence Research, Stanford pp. 99–108 (2014; also submitted to J. Comput. Phys.)
20. M. Brachet, D. Meiron, S. Orszag, B. Nickel, R. Morf, U. Frisch, J. Fluid Mech. **130**, 411 (1983)
21. N.D. Sandham, Q. Li, H.C. Yee, J. Comput. Phys. **178**, 307 (2002)
22. B. Sjögreen, H.C. Yee, J. Sci. Comput. **20**, 211 (2004)
23. H.C. Yee, B. Sjögreen, Shock Waves **17**, 185 (2007)
24. H.C. Yee, B. Sjögreen, A. Hadjadj, Commun. Comput. Phys. **12**, 1603 (2012)